OPEN ACCESS

ISAR Journal of Multidisciplinary Research and Studies
Abbriviate Tittle- ISAR J Mul Res Stud
ISSN *(Online)*- 2583-9705
https://isarpublisher.com/journal/isarjmrs

OPEN ACCESS

Numerical Investigation of a Blunt Body with Modified Aerospike in Drag Reduction

Pramod Chaudhary[1], Nikhil Kohar[2], Swaraj Chanda Joy[3]

[1, 2, 3] Aeronautical Engineering Department: Vel Tech Rangarajan & Dr. Sagunthala Institute of Science and Technology, Avadi, Chennai, India-600062.

***Corresponding Author**
Pramod Chaudhary

Aeronautical Engineering Department: Vel Tech Rangarajan & Dr. Sagunthala Institute of Science and Technology, Avadi, Chennai, India-600062.

Article History
Received: 04.10.2023
Accepted: 19.10.2023
Published: 20.11.2023

Abstract: *Aerospike installation on the forebody of a hypersonic rocket is one of the most challenging tasks. Small change in the structure may cause a great loss. This paper aims to design and develop an optimized structure of the aerospikes by varying the aerospike's frontal shape in order to reduce the drag acting on the forebody of a blunt nosed high-speed vehicle. The designs were done by using CATIA and the effect of air flowing over the blunt body are simulated numerically with the help of ANSYS Fluent.*

The simulations were carried out for different aerospike models by varying the aerodynamic structure of the aerospike. The coefficient of drag and its coefficients are estimated at zero-degree angle of attack and at a constant velocity of 1400 m/s by keeping pressure of 425 Pascal. Pressure contours and temperature contours are analyzed to find the pressure distribution and temperature distribution respectively. In addition, density and velocity contours are also studied. It is concluded from the results that the forebody with flat shape and cornered(fillet) edge aerospike model experienced less drag when compared with sharp edged and straight edged aerospike models.

Keywords: *aerospikes; CFD; cornered edge; fillet edge; sharp edge; drag; CATIA; ANSYS.*

INTRODUCTION

When a blunt body is introduced to hypersonic and supersonic flow, the formation of bow shock take place on the surface of the forebody. This shock wave is in the bow shape which results in raising the pressure over the surface of the body. Simultaneously, drag and its coefficient get increased which also led to foist the heating load on nose head of the body. This causes problem in the overall efficiency of the rocket due to high consumption of fuel even at low speed(Tekure, Pophali, & Venkatasubbaiah, 2021). So, to overcome these all problem, many research has been done and finally researcher came up with a new type of structure which is known as aerospike. This is designed to bear the pressure up to 60 psi and can invade into high flow speed(Z. Li, Sun, Xia, & Li, 2018; Xue, Wang, & Fu, 2018).

Aerospike is a structure which reduce the forebody pressure and aerodynamic drag of the blunt body at hypersonic and supersonic speed. When it attached on the forebody, it helps in flow separation at high speed due to its aerodynamic shape, which provide wide range to deviate the air flow at high speed and prevent the direct contact between airflow and forebody(Esfeh, Tajalli, & Liu, 2019). This suddenly helps to reduce the overall drag experienced by the rocket body while flying at speed of (2500-4500) m/s(Qin, Xu, & Guo, 2017; Sahoo, Karthick, Das, & Cohen, 2020).

Many researchers have developed different types of aerospikes and classified them on the basis of their shapes and structures. Some of the aerospikes based on the shape are mentioned below:

- Hemispherical aerospike
- Conical aerospike
- Flat shaped aerospike
- Blunt cone aerospike

Regarding all these aerospikes(Easwer, Manideep, & Kumar, 2023; Manigandan et al., 2019; Yadav, Bodavula, & Joshi, 2018), this research is based on Flat shaped aerospike which is also called backward facing aerospike. In the paper, the structure and shape of flat shaped aerospike has been modified into three different shapes. The shape is modified by changing the shape of their edge and they are given below:

A. Flat shape with sharp edge

In this shape, the angle between aerospike edge and strut is kept at 120°.

B. Flat shape with cornered edge

The Sharp is modified by applying one of the tool of the CATIA i.e., by cornering the new shape has been formed and the circle formed is at radius of 1mm.

C. Flat shape with straight edge

Instead of cornering, a straight line of 1 mm has been drawn from the edge of the spike and then by making the angle of 118°, edge is joined with strut.

Some of the researcher's view has mentioned below for the reference of this article.

1) Senthil Kumar S. et al(Senthilkumar, Mudholkar, & Sanjay, 2021)., numerically calculated the drag and its coefficient for a supersonic flow over the blunt body where he had compared three types of aerospikes i.e. Flat shaped aerospike, hemispherical aerospike and conical aerospikes at three angle of attack. It is found that when the flow becomes asymmetric due to increase in angle of attack, the lift coefficient is increased and the reduction of the drag take place. Hence, the flat shape aerospike has the highest drag reduction among all configurations.

2) Wan T et al.(Wan & Cm, 2017), had found out for spike off, the total drag is much higher than spike on case as a result of the presence of strong bow shock. In addition, the temperature distribution of the spike off is much higher than the spik on one. On the other hand, an innovative gap on the aero disk was proposed in his research and from the outcome, he argued that the minimum drag comes about the max gap under the same aerospike length.

3) Divyang Gupta et al(Pawar, Gilke, & Warade, 2018)., had numerically simulated hemispherical disk spike and flat triangular disk spike by using FVM. He investigated the influence of spike length and diameter of the disk and flow field visualization performed using velocity vector and contour plots. He concluded that the drag value is changing depends on the spike length and radius of the disk.

4) Saravanan et al(Narayan et al., 2019)., had experimentally verified the effectiveness of different types of forward-facing aerospikes for drag reductions at hypersonic speed. He concluded that for 120 apex angle blunt cone with forward facing aero disc, drag reduction of 40-55% has been measured for small angle of attack at normal Mach number. Spike without aero discs don't result in substantial reduction in drag.

This study shows the optimization of various shape in aerospikes. There are flat shape with sharp edge aerospike, flat shape with cornered aerospike and flat shape with straight edge aerospike. The CFD analysis is performed for above aerospikes to determine the coefficient of drag, temperature, pressure, density and velocity distribution over the surface of aerospikes with the input of 1400 m/s velocity and 425 pascals pressure as their boundary condition(Zhao et al., 2021).

Numerical Methodology

A. Governing Equation

For the analysis of a hypersonic flow past aerospikes with various length-to-diameter ratios, numerical simulations were generated. The governing equations are solved in their steady version since the current issue is steady. The two-equation standard k ε-model and a three-dimensional, stable, Reynolds-averaged Navier- Stokes equation are both solved in the current investigation(Bissuel, Allaire, Daumas, Barré, & Rey, 2018; Tsai, 2018). The ideal-gas equation of state completes the equation system(Abro, 2022; Kaushik, 2019; Marqués & Da Ronch, 2017; Schmitz, 2020). The following are the governing equations utilized for the numerical simulation:

1) Continuity Equation

$\partial\rho/\partial t + \nabla \cdot (\rho v) = 0$ (1)(Hansen, 2023; L. Li & Wang, 2021; Rizvi, 2017)

2) Momentum Equation

$\rho(\partial v/\partial t + v \cdot \nabla v) = -\nabla p + \mu\nabla^2 v + f$ (2)(Constantin, Drivas, Nguyen, & Pasqualotto, 2020; HUSSEİN, AZZİZ, & RASHİD, 2021; Kuya, Totani, & Kawai, 2018)

3) Energy Equation

$\rho(\partial e/\partial t + v \cdot \nabla e) = -p\nabla \cdot v + \nabla \cdot (k\nabla T) + \sigma$ (3)(Kuya et al., 2018; Refaie, Hameed, Nawar, Attai, & Mohamed, 2022; Yu, 2017)

where, ρ is the density of the fluid, t is time, v is the velocity vector of the fluid, ∇ is the divergence operator, p is the pressure of the fluid, μ is the dynamic viscosity of the fluid, ∇^2 is the Laplacian operator, which is a mathematical operator that measures the curvature of a scalar field, f represents any external forces acting on the fluid, such as gravitational or electromagnetic forces, k is the thermal conductivity of the fluid, T is the temperature of the fluid, σ is the rate of energy transfer due to viscous dissipation.

B. Model Geometry

This section illustrates the computer aided design (CAD) of the aerospikes with their shape optimization in the top portion of aerospike by making constraint to their base diameter of forebody is 50 mm and length of aerospike is 100 mm(Adaikalaraj, Sundararaj, & Syedhaleem, 2019). These constraints helps to depict the effect of flow separation and coefficient of drag due to the shape optimization in top portion (spike) of aerospikes. The CAD model of aerospikes were designed with the help of 3D-software named as CATIA for further analysis(Kim, 2017; Körber & Frommel, 2019). The aerospikes CAD model are shown in Figure 1.

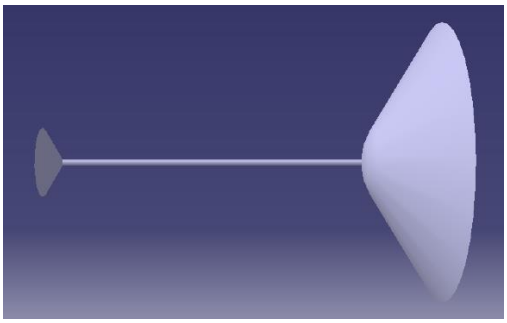

(a)

(b)

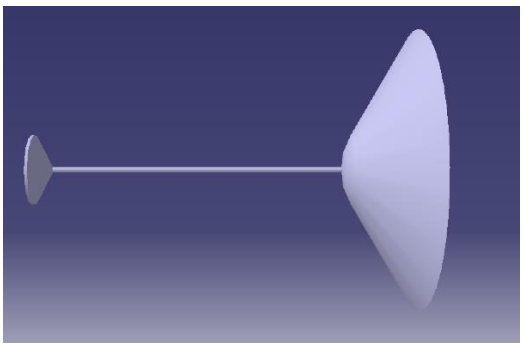

(c)

Figure 1. Shows the CAD model of three different aerospikes with L/D is 2. (a) shows flat shape with sharp edge aerospike; (b) shows flat shape with cornered edge aerospike; (c) shows flat shape with straight edge aerospike

The above geometries are the model of the aerospikes that mentioned earlier are designed in CATIA V5(El-Dahr, 2019). These aerospikes have different type of shape on the edge, which make them unique from each other. Fig.(a), shows Sharp edge having spike diameter of 25 mm, the distance between spike and forebody is 100 mm whereas the diameter of the forebody is taken as 100 mm and the angle between edge and strut is 120°. Similarly, for fig.(b) i.e., cornered edge is corner by 1 mm which provide blunted structure at the edge. In addition, all the dimension is same as Sharp edge. Likewise, Fig.(c) describes about the straight edge. Instead of Sharp edge, from the edge a straight line of 1 mm has been drawn which makes the angle between edge and strut of 118°.

The orthographic projection of the three modified type of the aerospikes are given below(Zhang et al., 2023):

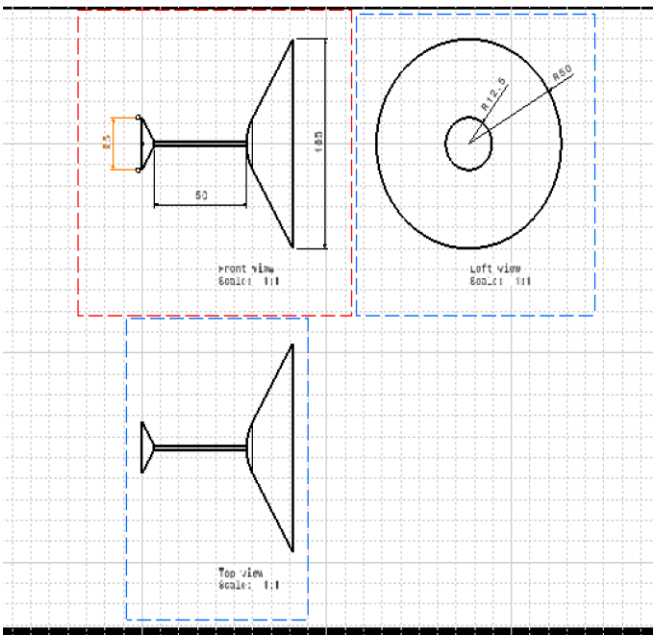

(a)

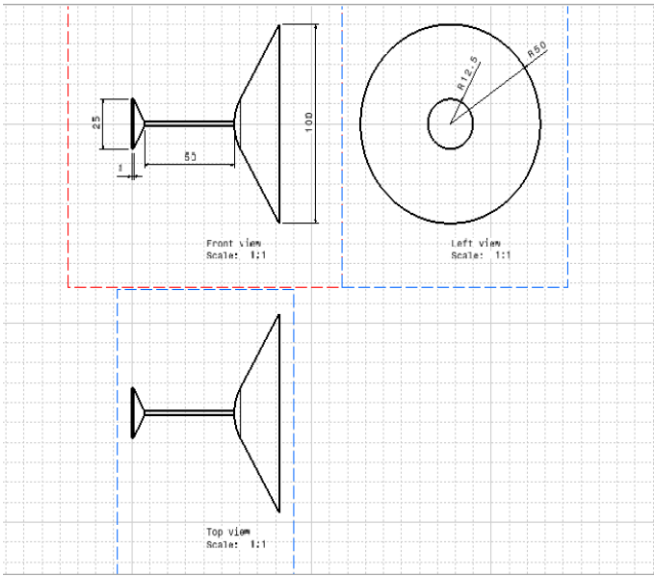

(b)

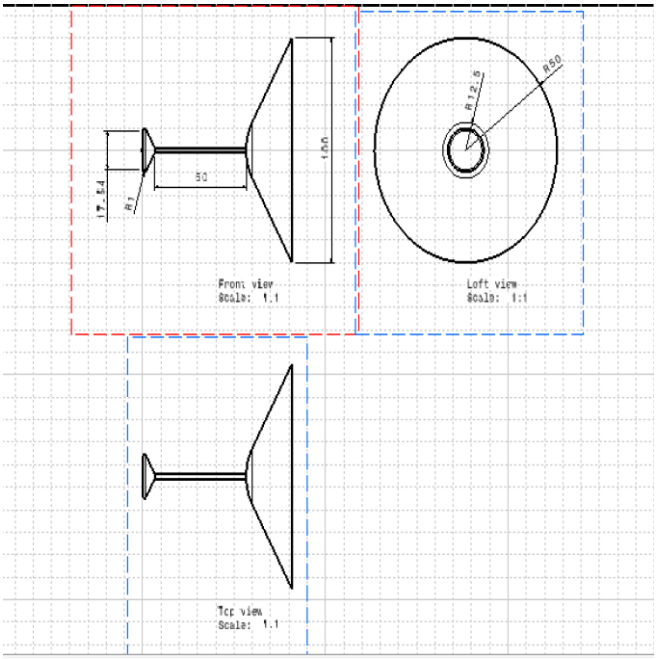

(c)

Figure 2. Shows the orthographic projection of above CAD model of three different aerospikes with L/D is 2. (a) shows flat shape with sharp edge aerospike; (b) shows flat shape with straight edge aerospike; (c) shows flat shape with cornered edge aerospike

C. Grid Generation and Meshing

Meshing is the important step in CFD analysis of any object so, finding the best mesh element size needs performing the grid independence test before meshing(Sosnowski, Krzywanski, Grabowska, & Gnatowska, 2018; Sosnowski, Krzywanski, & Scurek, 2019). The grid independence test has been carried out for x-velocity of an aerospike with mesh sizes ranging from 10mm to 20mm(M. Lee, Park, Park, & Kim, 2020; Mansour & Laurien, 2018). The number of elements and nodes for mesh sizes ranging from 10mm to 20mm is shown below in Table 1. These mesh size and elements are used to determine the grid independence test that

shows the best element size we have to select for CFD analysis which is clearly shown in graph in Figure 2.

Table 1. Grid independence test: Number of mesh elements with various element sizes ranging from 10 mm to 20 mm.

No. of Test	Independence Grid test		
	Mesh Element Size	No. of mesh nodes	No. of mesh element
1.	20	56800	56256
2.	19	60656	60096
3.	18	66284	65696
4.	17	74812	74192
5.	16	81284	80640
6.	15	91560	90880
7.	14	103844	103120
8.	13	120328	119552
9.	12	136936	136112
10.	11	162068	161168
11.	10	193412	192432

The grid refers to the set of interconnected nodes and elements that make up the finite element model. The grid defines the geometry of the model, as well as the material properties and boundary conditions that are applied to the model. The quality of the grid is critical to the accuracy and efficiency of the simulation results. A well-constructed grid should accurately capture the geometry of the model and the behaviour of the materials being analysed. It should also be fine enough to capture small-scale details, but not so fine that it significantly increases the computational cost of the simulation(Kummitha, 2017). The grid independence test outcomes are shown in Figure 3. It is clear from the observations that for a mesh element size of 13 mm, the result is stable, and the mesh element size of 13 mm can be taken into the meshing step for the CFD analysis. For subsequent CFD studies, a mesh element size of 11 mm can be used for higher precision.

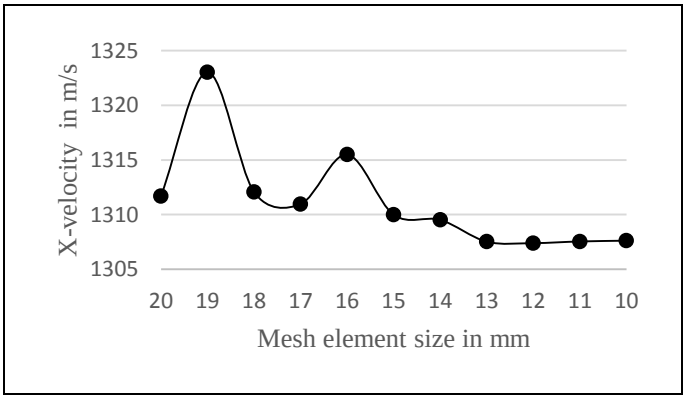

Figure 3. Shows the outcomes of grid independence test

The tetrahedral mesh elements are used in the meshing. Figure.4 (a) shows the complete meshed model, and Figure.4 (b) shows the enlarged view of the aerospike geometry. In this step, we choose fined mesh with refinement ratio of two that makes the meshing more accurate and precise. The value of elemental quality is 0.93 which shows accuracy of the mesh which is acceptable for further analysis.

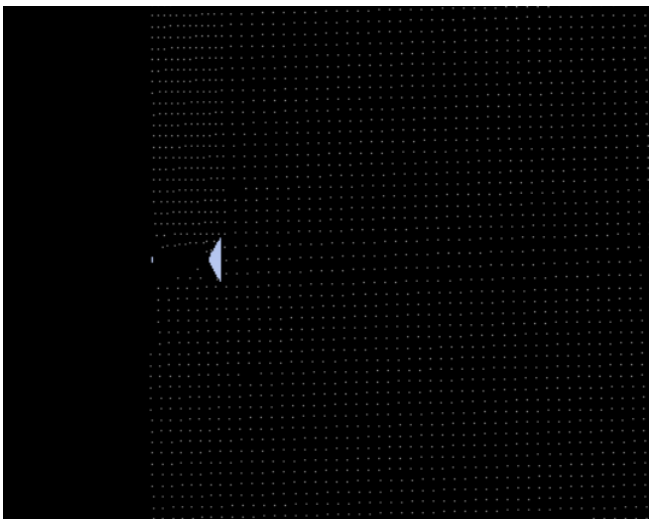

(a)

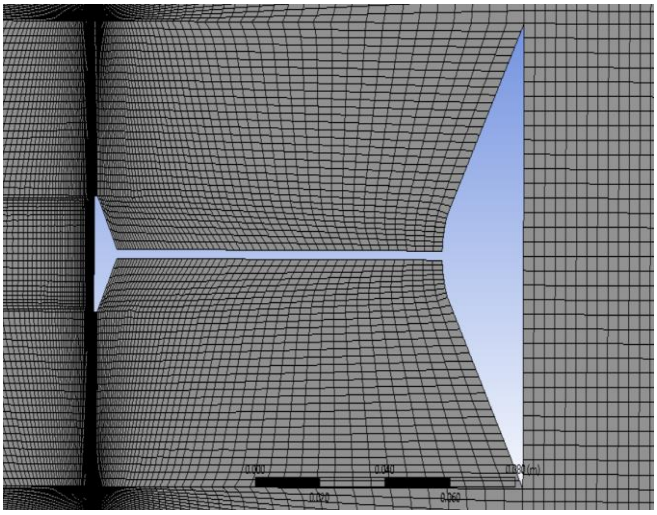

(b)

Figure 4. Meshed model of aerospike: (a) complete meshed aerospike; (b) Enlarged view of aerospike geometry

D. Flow Solver and Boundary Conditions

While doing the simulation, Density based solver is used which enables Navier-Stocks Coupled solution algorithm based on density where as k-epsilon with Standard Wall Function taken as viscous model(Afshari et al., 2018; Zawawi et al., 2018). Likewise, the free stream velocity is considered as inlet where the flow of fluid is given at 1400 m/s having pressure of 425 Pascal with wall temperature of 140 k. More ever, second order upwind is taken in spatial discretization for the turbulent kinetic energy and turbulent dissipation rate. For controlling the solution, the effective and precise courant number is taken as 0.7 with turbulent kinetic energy of 0.8. The residual criteria of this simulation is set to the value of 0.0001.

Results and Discussions

A. Flow visualization

Using numerical simulation of the flow around the spiky blunt body(H.-H. Lee, 2018; Van Thang, Vinh, Tri, & Trong, 2018), it has been demonstrated that a strong bow shock is produced at a short distance upstream of the body. Using an aerospike result in flow separation. The flow field around the nose cone is altered by

the addition of an aerospike. These figures demonstrate the formation of a bow shock in front of the aerospike, which has a substantial impact on the flow field in the recirculation zones.

1) Velocity contour of all three aerospikes

Velocity contour of aerospike with sharp edge, cornered edge and straight edge aerospikes are shown below. The high jet flow air strikes on the spike which creates the separation of flow and there is smooth flow of air in figure 5 (c) comparison to other aerospikes and thus the velocity distribution is more visible than other aerospikes.

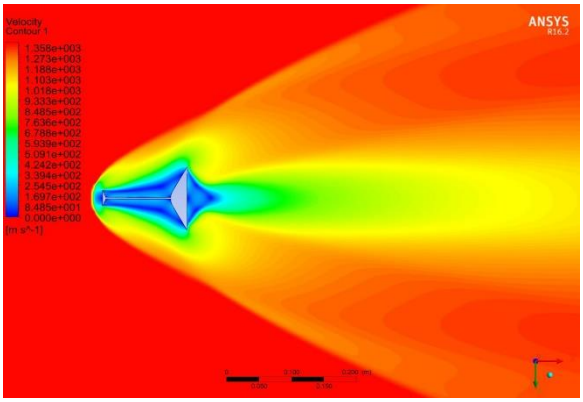

(a)

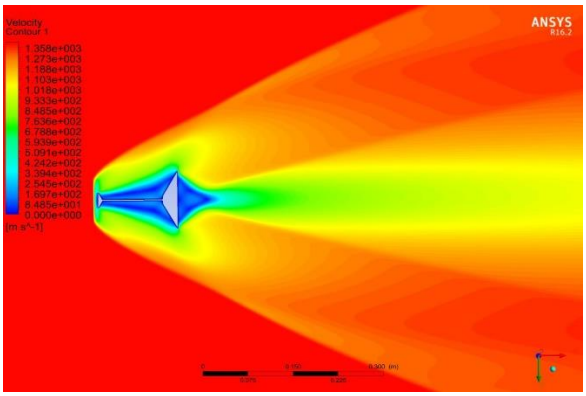

(b)

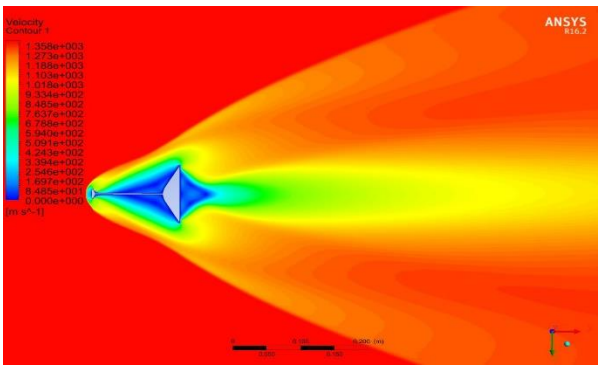

(c)

Figure 5. Velocity contour of three aerospikes: (a) velocity contour of Sharp edge spike; (b) Velocity contour of straight edge spike; (c) Velocity contour of cornered edge spike

2) Pressure contour of all three aerospikes

The distribution of pressure over the surface of sharp edge aerospike, straight edge aerospike and cornered edge aerospike are clearly observed in pressure contour of all aerospikes. The formation of bow shock wave is weak in figure 6 (c). The strong bow shock wave is detached in cornered edge aerospike, makes the flow smooth, and thus reduces the coefficient of drag.

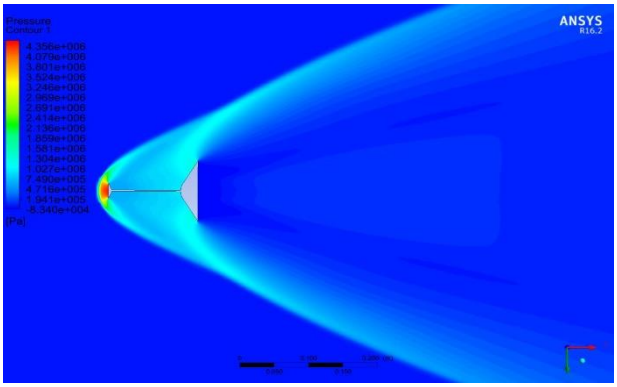

(a)

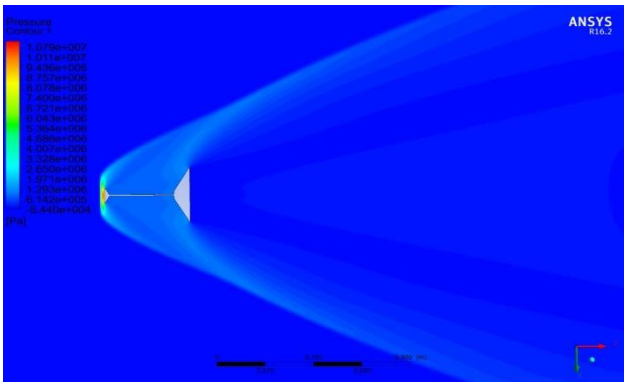

(b)

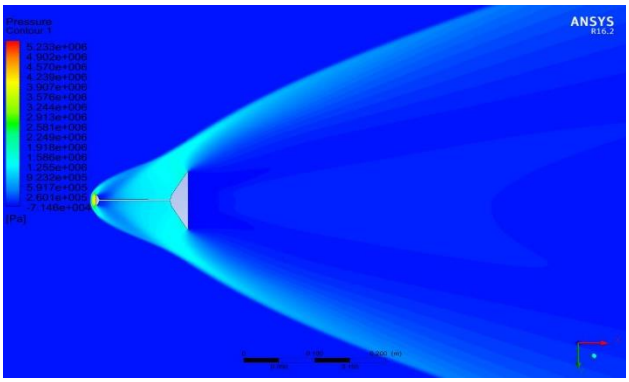

(c)

Figure 6. Pressure contour of three aerospikes: (a) Pressure contour of Sharp edge spike; (b) Pressure contour of straight edge spike; (c) Pressure contour of cornered edge spike

3) Density Contour of all three aerospikes

The distribution of density over the surface of three aerospike are shown below. We can see the varying of density at different point like on the edge of aerospike. At the edge, there is more compression of the high-speed air flow and after onward rarefaction take place. The density distribution in figure 7 (c) is more dense and smooth than figure 7 (a) and figure 7 (b).

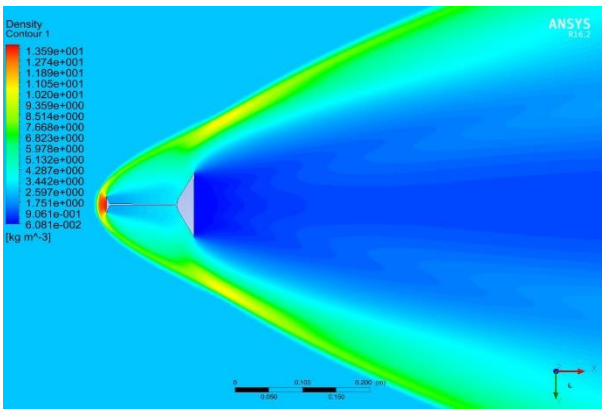

(a)

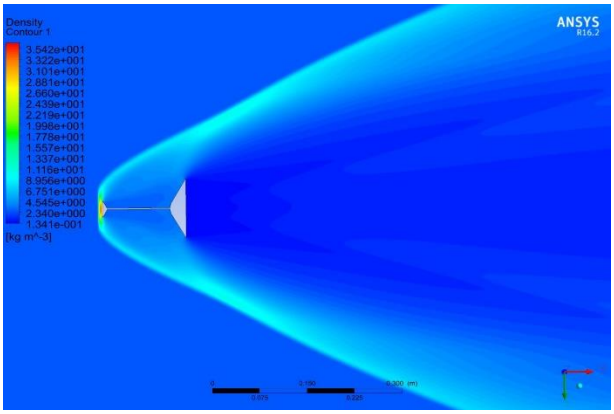

(b)

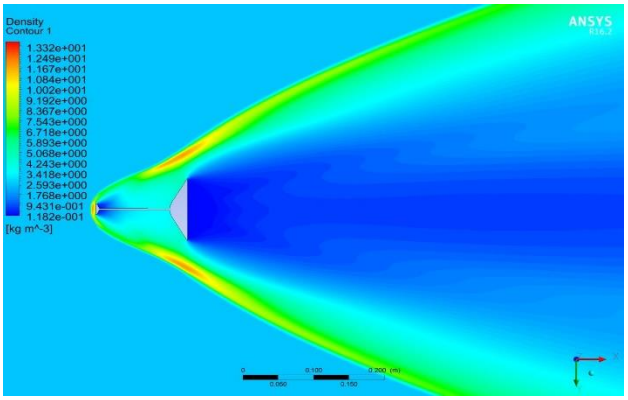

(c)

Figure 7. Density contour of three aerospikes: (a) Density contour of Sharp edge spike; (b) Density contour of straight edge spike; (c) Density contour of cornered edge spike

4) Temperature contour of all aerospikes

Temperature distribution over the surface of three aerospike are shown below. The temperature distribution varies from tip of the aerospike to the forebody of the aerospike. The temperature distribution is more smooth and low in figure 8 (c) as compared to the figure 8 (a) and figure 8 (b). The aerospike having low temperature distribution is suited for designing aerospike to reduce aerodynamic heating and thus reduce drag.

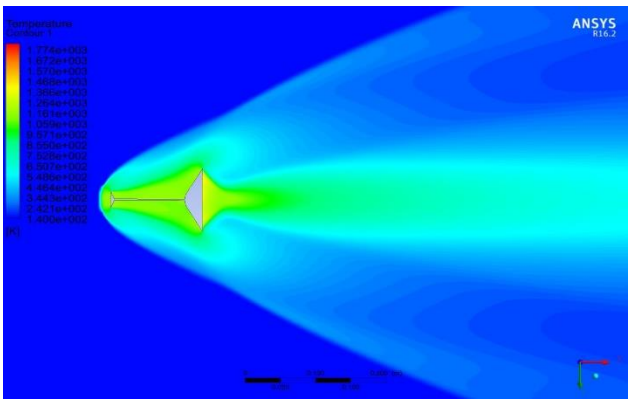

(a)

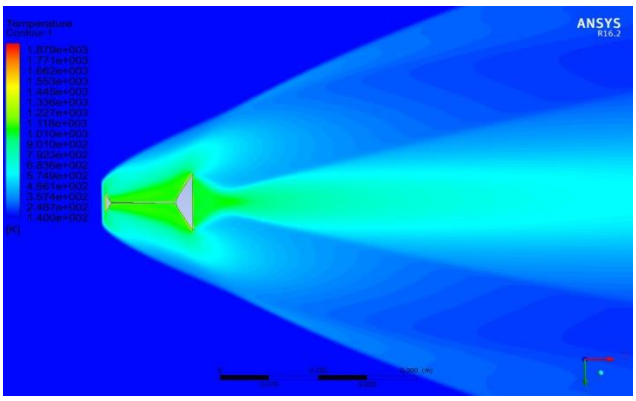

(b)

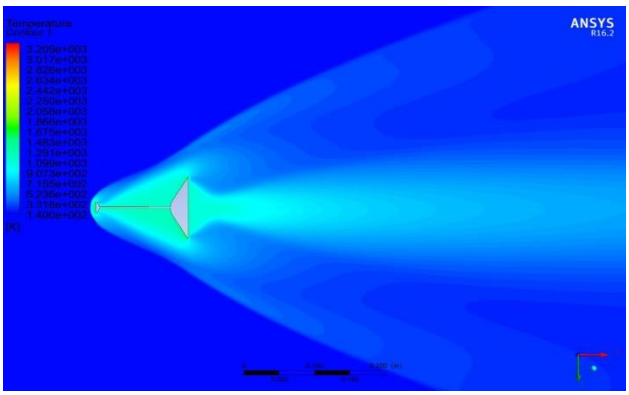

(c)

Figure 8. Temperature contour of three aerospikes: (a) Temperature contour of Sharp edge spike; (b) Temperature contour of straight edge spike; (c) Temperature contour of cornered edge spike

B. Drag Reduction

While comparing the values of drag and its coefficient calculated from simulation, it is analyzed that there is good drag reduction on the aerospike with cornered edge than other aerospike i.e., aerospike with Sharp edge and straight edge. By using below equation, the coefficient of drag were calculated(Eghlima & Mansour, 2017; Gerdroodbary, 2022);

$$C_d = \frac{F_d}{(\mathbf{qref} * \mathbf{S})}$$

Where, F_d is drag force exerted on the body, qref is the dynamic pressure and S is the reference area of the body.

Table 2. Comparison of coefficient of drag

S.N.	Types of Aerospikes	Coefficient of Drag (Cd)
1.	Flat shaped aerospikes with sharp edge (G. Jagadeesh)	1.12
2.	Flat shaped aerospike with Sharp edge	1.05
3.	Flat shaped aerospike with straight edge	1.13
4.	Flat shaped aerospike with cornered edge	0.69

From this given table, Cd value is compared and validated with the experimental value of G. Jagadeesh(Deep & Jagadeesh, 2018). Likewise, it is concluded that the aerospike having cornered edge is considered as the most efficient one. It exerted less coefficient of drag among the other aerospikes.

C. Pressure Distribution

While introducing the aerospike over the nose of blunt body, the flow field got changed which result in reducing the pressure. Hence, the flow gets decelerated and the coefficient of pressure can be calculated by using the given formula:

$$Cp = \frac{\mathbf{P - Pref}}{\mathbf{qref}}$$

Where, qref is the dynamic pressure, Pref is free stream pressure and p is the pressure at the given point(Gerhart, Hochstein, & Gerhart, 2020; Sasoh, 2020).

D. Temperature Distribution

From the above contour, it is found that the distribution of temperature gets enhanced while using the aerospikes. More ever, the aerospike with cornered edge normalized the values of temperature by dividing them with stagnation temperature(Qin et al., 2017).

Conclusion

Numerical investigation on different shape and structure of aerospikes has been performed which showed the variation of the drag and its coefficient regarding the shapes of the aerospikes. Hence, it is concluded that maximum drag reduction takes place on the forebody which attached with flat shaped aerospike with cornered edge where the length between aerospike and forebody is taken in L/D ratio i.e., 2 and the free stream velocity is given as inlet having flow speed of 1400 m/s. Likewise, the inlet pressure is maintained at 425 Pascal with temperature of 140 k. The value of coefficient of drag in cornered edge aerospike from the numerical simulation is 0.69 which is less than sharp edge aerospike having Cd 1.05 and straight edge aerospike having Cd 1.13. The simulation clearly showed the domination of Cornered edge aerospike over the aerospike having sharp edge and straight edge while calculating the drag and its coefficient.

Funding

Acknowledgements

We are thankful to the Research team of the Aeronautical Engineering Department of Vel Tech Rangarajan Dr. Sagunthala Institute of Science and Technology, Avadi, Chennai, India-600062 under the supervision of Associate professor Dr. R. Naren Sankar and their cooperation and support throughout the research period.

Author contributions

Conceptualization, P.C and N.K; methodology, N.K, S.C.J and P.C, software, P.C; validation, P.C, N.K and S.C.J; formal analysis, P.C; investigation, P.C, N.K and S.C.J; resources, S.C.J, P.C and N.K; data curation, P.C, and N.K; writing- Original draft preparation P.C and N.K; writing - Review and editing, P.C. All authors have read and agreed to the published version of the manuscript.

Conflict of interest

The authors declare no conflict of interest.

REFRANCES

1. Abro, K. A. (2022). Numerical study and chaotic oscillations for aerodynamic model of wind turbine via fractal and fractional differential operators. *Numerical Methods for Partial Differential Equations*, *38*(5), 1180-1194.
2. Adaikalaraj, A., Sundararaj, M., & Syedhaleem, M. (2019). Computational Analysis of Flow over Bluff Bodies using Aero Spikes. *International Journal of Vehicle Structures & Systems (IJVSS)*, *11*(2).
3. Afshari, F., Zavaragh, H. G., Sahin, B., Grifoni, R. C., Corvaro, F., Marchetti, B., & Polonara, F. (2018). On numerical methods; optimization of CFD solution to evaluate fluid flow around a sample object at low Re numbers. *Mathematics and Computers in Simulation*, *152*, 51-68.
4. Bissuel, A., Allaire, G., Daumas, L., Barré, S., & Rey, F. (2018). Linearized Navier–Stokes equations for aeroacoustics using stabilized finite elements: Boundary conditions and industrial application to aft-fan noise propagation. *Computers & Fluids*, *166*, 32-45.
5. Constantin, P., Drivas, T. D., Nguyen, H. Q., & Pasqualotto, F. (2020). *Compressible fluids and active potentials.* Paper presented at the Annales de l'Institut Henri Poincaré C, Analyse non linéaire.
6. Deep, S., & Jagadeesh, G. (2018). Aerothermodynamic effects of controlled heat release within the hypersonic shock layer around a large angle blunt cone. *Physics of Fluids*, *30*(10).
7. Easwer, D., Manideep, B., & Kumar, A. S. (2023). *Numerical simulation of a blunt body to investigate drag characteristics with active and passive device.* Paper presented at the AIP Conference Proceedings.

8. Eghlima, Z., & Mansour, K. (2017). Drag reduction for the combination of spike and counterflow jet on blunt body at high Mach number flow. *Acta Astronautica, 133*, 103-110.

9. El-Dahr, B. (2019). PERFORMANCE TRENDS FOR AEROSPIKES & SUPERSONIC NOZZLES WITH CENTER-BODIES.

10. Esfeh, M. K., Tajalli, S. M., & Liu, P. (2019). Evaluation of aerospike for drag reduction on a blunt nose using experimental and numerical modeling. *Acta Astronautica, 160*, 656-671.

11. Gerdroodbary, M. B. (2022). *Aerodynamic heating in supersonic and hypersonic flows: advanced techniques for drag and aero-heating reduction*: Elsevier.

12. Gerhart, A. L., Hochstein, J. I., & Gerhart, P. M. (2020). *Munson, Young and Okiishi's fundamentals of fluid mechanics*: John Wiley & Sons.

13. Hansen, A. H. (2023). Fluids Mechanics. In *Fluid Power Systems: A Lecture Note in Modelling, Analysis and Control* (pp. 25-42): Springer.

14. HUSSEİN, E., AZZİZ, H., & RASHİD, F. (2021). Aerodynamic study of slotted flap for NACA 24012 airfoil by dynamic mesh techniques and visualization flow. *Journal of Thermal Engineering, 7*(2), 230-239.

15. Kaushik, M. (2019). *Theoretical and experimental aerodynamics*: Springer.

16. Kim, G.-Y. (2017). Development of a software tool for automatic trim steel design of press die using CATIA API. *Journal of the Korea Academia-Industrial cooperation Society, 18*(3), 72-77.

17. Körber, M., & Frommel, C. (2019). Automated planning and optimization of a draping processes within the CATIA environment using a Python software tool. *Procedia Manufacturing, 38*, 808-815.

18. Kummitha, O. R. (2017). Numerical analysis of hydrogen fuel scramjet combustor with turbulence development inserts and with different turbulence models. *International Journal of hydrogen energy, 42*(9), 6360-6368.

19. Kuya, Y., Totani, K., & Kawai, S. (2018). Kinetic energy and entropy preserving schemes for compressible flows by split convective forms. *Journal of Computational Physics, 375*, 823-853.

20. Lee, H.-H. (2018). *Finite element simulations with ANSYS Workbench 18*: SDC publications.

21. Lee, M., Park, G., Park, C., & Kim, C. (2020). Improvement of grid independence test for computational fluid dynamics model of building based on grid resolution. *Advances in Civil Engineering, 2020*, 1-11.

22. Li, L., & Wang, J. (2021). Nanosecond dielectric barrier discharge on a curved surface in atmospheric air: streamer evolution and aerodynamic perturbations. *Journal of Physics D: Applied Physics, 55*(5), 055203.

23. Li, Z., Sun, C., Xia, X., & Li, X. (2018). Numerical simulation of aerodynamic heating over solid blunt configuration with porous spike. *Journal of Aerospace Engineering, 31*(6), 04018083.

24. Manigandan, S., Sruthisree, K., Aich, K., Gunasekar, P., Nithya, S., Devipriya, J., & Venkatesh, S. (2019). *Numerical analysis of slotted aerospike for drag reduction.* Paper presented at the Journal of Physics: Conference Series.

25. Mansour, A., & Laurien, E. (2018). Numerical error analysis for three-dimensional CFD simulations in the two-room model containment THAI+: Grid convergence index, wall treatment error and scalability tests. *Nuclear Engineering and Design, 326*, 220-233.

26. Marqués, P., & Da Ronch, A. (2017). *Advanced UAV aerodynamics, flight stability and control: novel concepts, theory and applications*: John Wiley & Sons.

27. Narayan, A., Narayanan, S., Kumar, R., Singh, T., Kumar, C., & Jagadeesh, G. (2019). Control of aerodynamic drag and heating of nose cones through taper spikes. *Journal of Spacecraft and Rockets, 56*(4), 1165-1176.

28. Pawar, R. S., Gilke, N., & Warade, V. P. (2018). *Numerical Simulation Over Flat-Disk Aerospike at Mach 6.* Paper presented at the 2018 IEEE International Conference on System, Computation, Automation and Networking (ICSCA).

29. Qin, Q., Xu, J., & Guo, S. (2017). Fluid-thermal analysis of aerodynamic heating over spiked blunt body configurations. *Acta Astronautica, 132*, 230-242.

30. Refaie, A. G., Hameed, H. A., Nawar, M. A., Attai, Y. A., & Mohamed, M. H. (2022). Comparative investigation of the aerodynamic performance for several Shrouded Archimedes Spiral Wind Turbines. *Energy, 239*, 122295.

31. Rizvi, Z. A. (2017). A study to understand differential equations applied to aerodynamics using CFD technique. *International Journal of Scientific & Engineering Research*, *8*(2), 16-19.

32. Sahoo, D., Karthick, S. K., Das, S., & Cohen, J. (2020). Parametric experimental studies on supersonic flow unsteadiness over a hemispherical spiked body. *AIAA Journal*, *58*(8), 3446-3463.

33. Sasoh, A. (2020). Compressible fluid dynamics and shock waves.

34. Schmitz, S. (2020). *Aerodynamics of wind turbines: a physical basis for analysis and design*: John wiley & sons.

35. Senthilkumar, S., Mudholkar, A. A., & Sanjay, K. (2021). *A Comparative Study on Aerodynamic Drag Reduction of a Blunt Nose Body using Aerospike and Aerodisk–Numerical Approach*. Paper presented at the IOP Conference Series: Materials Science and Engineering.

36. Sosnowski, M., Krzywanski, J., Grabowska, K., & Gnatowska, R. (2018). *Polyhedral meshing in numerical analysis of conjugate heat transfer*. Paper presented at the EPJ Web of Conferences.

37. Sosnowski, M., Krzywanski, J., & Scurek, R. (2019). A fuzzy logic approach for the reduction of mesh-induced error in CFD analysis: A case study of an impinging jet. *Entropy*, *21*(11), 1047.

38. Tekure, V., Pophali, P. S., & Venkatasubbaiah, K. (2021). Numerical investigation of aerospike semi-cone angle and a small bump on the spike stem in reducing the aerodynamic drag and heating of spiked blunt-body: New correlations for drag and surface temperature. *Physics of Fluids*, *33*(11).

39. Tsai, T.-P. (2018). *Lectures on Navier-Stokes equations* (Vol. 192): American Mathematical Soc.

40. Van Thang, N., Vinh, H. T., Tri, B. D., & Trong, N. D. (2018). Numerical simulation of airflow around vehicle models. *Vietnam Journal of Science and Technology*, *56*(3), 370-379.

41. Wan, T., & Cm, L. (2017). Drag reduction optimization for hypersonic blunt body with aerospikes. *Journal of Aeronautics & Aerospace Engineering*.

42. Xue, Y., Wang, L., & Fu, S. (2018). Drag reduction and aerodynamic shape optimization for spike-tipped supersonic blunt nose. *Journal of Spacecraft and Rockets*, *55*(3), 552-560.

43. Yadav, R., Bodavula, A., & Joshi, S. (2018). Numerical investigation of the effect of disk position on the aerodynamic heating and drag of a spiked blunt body in hypersonic flow. *The Aeronautical Journal*, *122*(1258), 1916-1942.

44. Yu, C. (2017). Energy conservation for the weak solutions of the compressible Navier–Stokes equations. *Archive for Rational Mechanics and Analysis*, *225*(3), 1073-1087.

45. Zawawi, M. H., Saleha, A., Salwa, A., Hassan, N., Zahari, N. M., Ramli, M. Z., & Muda, Z. C. (2018). *A review: Fundamentals of computational fluid dynamics (CFD)*. Paper presented at the AIP conference proceedings.

46. Zhang, C., Pinquié, R., Polette, A., Carasi, G., De Charnace, H., & Pernot, J.-P. (2023). Automatic 3D CAD models reconstruction from 2D orthographic drawings. *Computers & Graphics*.

47. Zhao, H., Peng, K., Wu, Z., Zhang, W., Yang, J., & Sun, J. (2021). Numerical simulation of supersonic Carman curve bodies with aerospike. *International Journal of Aerospace Engineering*, *2021*, 1-14.

.